International Journal of Research in Engineering

E-ISSN: 2664-8784
P-ISSN: 2664-8776
IJRE 2024; 6(1): 04-16

www.engineeringpaper.net
Received: 07-11-2023
Accepted: 09-12-2023
Published: 06-02-2024

Ahmed Hashim Kareem
Department of Mechanical, Amarah Technical Institute, Southern Technical University, Iraq

Correspondence
Ahmed Hashim Kareem
Department of Mechanical, Amarah Technical Institute, Southern Technical University, Iraq

Study and analysis of contact stresses in spur gears by finite element method

Ahmed Hashim Kareem

DOI: https://dx.doi.org/10.33545/26648776.2024.v6.i1a.49

Abstract
A finite element simulation for surface contact stresses of gear teeth is presented. The derivation of finite element equations based on elastic large deflection. Main outlines for a finite element solution algorithm and software are given for this purpose, due to stability and measuring accuracy problems an existing finite element-package is used. In this study five positions along the contact line are considered to evaluate the contact stress on the pinion and wheel teeth. The influence of speed ratio and ratio of Young's modulus of the pinion are considered during the investigation. Found that the maximum shear stress is the beginning and the end from contact point, therefore the design life calculations of the gear tooth should be based upon these points instead of the pitch point of contact stress in the systemic design calculations. Values of the depth with shifting depended upon the position of contact point along the pressure line.

Keywords: Spur gear, Contact ratio, Contact stress, FEM

Introduction

Predict the stresses and deformations when the surfaces of two solid bodies are brought into contact, subject to the surface of constraints. Solids touching each other are deformable at one or the more points.

Shiferaw Damtie and Daniel Tilahun [1]. Studied the coefficient of friction and its effect on contact stress by using both FEM and Hertizian stress formula. Where it was found that the higher the coefficient of friction, the contact stress increases. Ali Raad Hassan [2] use the finite element method for the contact stress analysis, different contact positions at the two spurs gears. Keer LM and Bryant MD [3] studied apply fracture mechanics to pit formation mechanisms. They found that the pitting phenomenon strongly depends on the contact surface. Rao *et al.* [4] used the FEM for contact stress analysis in mating gears. Research aims for reduced both contact stress and deformation. Zhai [5]. Derived the contact stress on the tooth surface by using contact theory. Using FE simulation analysis, the contact stresses are calculated of the tooth surface. Flasker *et al.* [6] a new model is the described to simulate the surface stress process in contact of the area for the spur gears. SIVAKUMAR *et al.* [7]. Used the numerical analysis to find contact stress with bending stress for gears and pinion by using ANSYS. Hertz's equations are used to analysis contact stresses. Narayankar and Mangrulkar [8] Derived the bending and contact stresses by using Hertzian and Lewis equations. Abbasi *et al.* [9] A new strategy for seamless two dimensional contact surface representation and implementation has been developed. Balaji *et al.* [10]. Examined the contact stress by using Hertzian equation. Through numerical analysis, both contact and bending stresses are calculated using the ANSYS program. Results from the theoretical analysis are compared to the results for FE analysis. Glodez *et al.* [11] studied a two-dimensional of the computational model to the simulate the surface, which resulted in the growth of fatigue cracks in the contact area of the tips of the gear teeth resulting in surface pitting. Selvam *et al.* [12] Studied and developed the bending stress under a spur gear pair by using both the theoretical and FE analysis methods. Xiaoyn Lei [13] presented a simple interface element for analyzing contact friction problems developed in this work. Francvilla and Zienkiewicz [14] Presented for simple procedure for the obtaining elasticity matrices in terms of the contact pressure for the potential contact points of two bodies. Glodez *et al.* [15]. The two-dimensional computational model has been studied, and it has been limited to the modeling of high-precision mechanical components.

Finite element method theory

The FE methods are techniques for approximating the govering differential equations for a continuum with a set of algebraic equations relating a finite number of variables.

State of stress

For the stresses in the internal point of the body for 3D analysis is given as by:

$$\begin{bmatrix} \sigma \end{bmatrix} = \begin{bmatrix} \sigma_x & \tau_{yx} & \tau_{zx} \\ \tau_{xy} & \sigma_y & \tau_{zy} \\ \tau_{xz} & \tau_{yz} & \sigma_z \end{bmatrix} \tag{1}$$

Where stress components must satisfy of the following equilibrium of equations through the interior of the body.

$$\frac{\partial \sigma_x}{\partial x} + \frac{\partial \tau_{xy}}{\partial y} + \frac{\partial \tau_{xz}}{\partial z} + Fx = 0 \tag{2}$$

$$\frac{\partial \tau_{xy}}{\partial x} + \frac{\partial \sigma_y}{\partial y} + \frac{\partial \tau_{yz}}{\partial z} + Fy = 0 \tag{3}$$

$$\frac{\partial \tau_{xz}}{\partial x} + \frac{\partial \tau_{yz}}{\partial y} + \frac{\partial \sigma_z}{\partial z} + Fz = 0 \tag{4}$$

Where F_x, F_y, F_z are body forces of components per unit volume and for 2D problems, the Z components vanish.

State of strains and displacements boundary conditions

State of the strains at the point inside of loaded body is given by as following:

$$[\varepsilon] = \begin{bmatrix} \varepsilon_x & \gamma_{xy} & \gamma_{xz} \\ \gamma_{xy} & \varepsilon_y & \gamma_{yz} \\ \gamma_{xz} & \gamma_{yz} & \varepsilon_z \end{bmatrix} \tag{5}$$

Strain-displacement relations from the small deflection theory are:

$$\gamma_{xy} = \left(\frac{\partial u}{\partial y} + \frac{\partial v}{\partial x} \right) \tag{7}$$

$$\gamma_{xy} = \left(\frac{\partial w}{\partial y} + \frac{\partial v}{\partial z} \right) \tag{8}$$

$$\gamma_{xy} = \left(\frac{\partial u}{\partial z} + \frac{\partial w}{\partial x} \right) \tag{9}$$

If Γu denotes the portion for the boundary surface on which the displacements are prescribed. Displacement constraints are:

$$u = \bar{u} \qquad , v = \bar{v}, \qquad w = \bar{w} \tag{10}$$

Where $\bar{u}$, $\bar{v}$ & $\bar{w}$ are prescribed values and Γ_u is part of total boundary.

Stresses and strains relations
Linear elastic of the materials stresses-strains relations can be deduced from the generalized Hooke's law. Isotropic homogenous materials. Elemental cube inside of the body Hooke's law given as:

$$\varepsilon_x = \frac{\sigma_x}{E} - \upsilon\frac{\sigma_y}{E} - \upsilon\frac{\sigma_z}{E} \tag{11}$$

$$\varepsilon_y = -\upsilon\frac{\sigma_x}{E} + \frac{\sigma_y}{E} - \upsilon\frac{\sigma_z}{E} \tag{12}$$

$$\varepsilon_z = -\upsilon\frac{\sigma_x}{E} - \upsilon\frac{\sigma_y}{E} + \frac{\sigma_z}{E} \tag{13}$$

$$\gamma_{yz} = \frac{\tau_{yz}}{G}, \gamma_{xz} = \frac{\tau_{xz}}{G}, \gamma_{xy} = \frac{\tau_{xy}}{G} \tag{14}$$

The shear modulus G is given as:

$$G = \frac{E}{2(1+\upsilon)} \tag{15}$$

From Hooke's law relationships the equations (11),(12),(13) and (14), note that:

$$\varepsilon_x + \varepsilon_y + \varepsilon_z = \frac{(1-2\upsilon)}{E}\left(\sigma_x + \sigma_y + \sigma_z\right) \tag{16}$$

Substituting the $\left(\sigma_y + \sigma_z\right)$ and the equations (11),(12),(13) and (14), the inverse relations are obtained:

$$\underline{\sigma} = [D] * \underline{\varepsilon} \tag{17}$$

$[D]$: Symmetric (6*6) material matrix given as:

$$[\ D\ ] = \frac{E}{(1+\upsilon)(1-2\upsilon)}\begin{bmatrix} 1-\upsilon & \upsilon & \upsilon & 0 & 0 & 0 \\ \upsilon & 1-\upsilon & \upsilon & 0 & 0 & 0 \\ \upsilon & \upsilon & 1-\upsilon & 0 & 0 & 0 \\ 0 & 0 & 0 & 5-\upsilon & 0 & 0 \\ 0 & 0 & 0 & 0 & 5-\upsilon & 0 \\ 0 & 0 & 0 & 0 & 0 & 5-\upsilon \end{bmatrix} \tag{18}$$

For plane stress problems, where $\sigma_z = \tau_{xz} = \tau_{yz} = 0$, Hooke's law of the relations equations (11),(12),(13) and (14) is reduced to:

$$\varepsilon_x = \frac{\sigma_x}{E} - \upsilon \frac{\sigma_y}{E}$$

$$\varepsilon_y = -\upsilon \frac{\sigma_x}{E} + \frac{\sigma_y}{E} \qquad (19)$$

$$\gamma_{xy} = \frac{2(1+\upsilon)}{E}\tau_{xy}$$

$$\varepsilon_z = -\frac{\upsilon}{E}\left(\sigma_x + \sigma_y\right)$$

Inverse relations are given as:

$$\begin{Bmatrix} \sigma_x \\ \sigma_y \\ \tau_{xy} \end{Bmatrix} = \frac{E}{1-\upsilon^2}\begin{bmatrix} 1 & \upsilon & 0 \\ \upsilon & 1 & 0 \\ 0 & 0 & \dfrac{1-\upsilon}{2} \end{bmatrix}\begin{Bmatrix} \varepsilon_x \\ \varepsilon_y \\ \gamma_{xy} \end{Bmatrix} \qquad (20)$$

Which using as:

$$\underline{\sigma} = [D] * \underline{\varepsilon}$$

Principle of the virtual works

For the body in the equilibrium under external loading F_x, F_y, F_z, body forces, $\bar{P}_x, \bar{P}_y, \ldots\ldots$ external forces $\sigma_x, \sigma_y, \ldots\ldots\ldots \tau_{xy}$ internal stresses if the body is displaced from its equilibrium position virtually by $\Delta u, \Delta v, \Delta w$ virtual displacements, the body forces, external forces and internal forces do certain amount of the virtual works. According to principles of the virtual displacements total virtual work done by internal forces (due to stresses) W_D equal for virtual work done by external and body forces W_E.

$$W_D = W_E \qquad (21)$$

The three dimensional form equation (21) is

$$\iiint \left(\sigma_x\, \delta\varepsilon_x + \sigma_y\, \delta\varepsilon_y + \sigma_z\, \delta\varepsilon_z + \tau_{xy}\, \delta\varepsilon_{xy} + \tau_{xz}\, \delta\varepsilon_{xz} + \tau_{yz}\, \delta\varepsilon_{yz} + \right.$$
$$\left. \tau_{yx}\, \delta\varepsilon_{yx} + \tau_{zx}\, \delta\varepsilon_{zx} + \tau_{zy}\, \delta\varepsilon_{zy}\right) dx\ dy\ dz =$$
$$\iiint \left(F_x . \Delta u + F_y . \Delta v + F_z . \Delta w\right) dx . dy . dz \qquad (22)$$
$$+ \iint \left(P_x . \Delta u + P_y . \Delta v + P_z . \Delta w\right) ds$$

and in the matrix form

$$\iiint \underline{\sigma}^T . \underline{\delta\varepsilon} . dvol = \iiint \underline{F}^T . \underline{\Delta u} . dvol + \iint \underline{P}^T . \underline{\Delta u} . ds \qquad (23)$$

Equation (23) can be restated as:

$$\iiint \underline{\sigma}^{T} .\underline{\delta\varepsilon}.dvol - \left\lfloor \iiint \underline{F^{T}}.\underline{\Delta u}.dvol + \iint \underline{P^{T}}.\underline{\Delta u}.ds \right\rfloor = 0 \qquad (24)$$

The first term of the equation (24) can be recognized of the variation for strains energy $\overline{U}$ with second term as the variation of work done due to incremental displacements $\underline{\Delta U}$. If the work done is also expressed as a potential $\overline{W}$, then the equation (24) can be written as:

$$\delta\left(\overline{U} + \overline{W}\right) = \delta\left(\Pi\right) = 0 \qquad (25)$$

Where

Π : is the potential energy

Total potential energy for element.

$$\lambda = U - W$$

$$U = \frac{1}{2}\iiint \underline{\sigma}^{T}\ \underline{\varepsilon}\, dx.dy.dz \qquad (26)$$

$$W = \underline{\delta}^{T}.\underline{P}$$

But $[D]^{T} = [D]$ due to symmetry of the matrix and $\sigma^{T} = \delta^{T}.[B]^{T}.[D]$

Then

$$U = \frac{1}{2}\iiint \underline{\delta}^{T}\ [B]^{T}\ [D]\ [B]\ \underline{\delta}\, dx\ dy\ dz \qquad (27)$$

$$\lambda = U - W = \frac{1}{2}\underline{\delta}^{T}\left[\iiint [B]^{T}\ [D]\ [B]\ dx\ dy\ dz\right]\underline{\delta} - \underline{\delta}^{T}\ \underline{P} \qquad (28)$$

By applying minimum total of potential energy principle to equation (28), the following can be proved:

$$\frac{\partial\lambda}{\partial\delta} = 0 = \left[\iiint [B]^{T}\ [D]\ [B]\ dx\ dy\, dz\right]\underline{\delta} - \underline{P} = 0 \qquad (29)$$

$$= K_{e}\,\underline{\delta} = \underline{P}$$

Where K_{e} is the bracketed term in equation (29)

Since for two-dimensional case $[B]$ is independent of z, then

$$K_{e} = \left\lfloor \iint [B]^{T}.[D].[B].dA \right\rfloor .t \qquad (30)$$

t: the element of the thickness in z-direction.

$$dA = \left| J\left(\frac{x,y}{\xi,\eta}\right)\right| .d\xi.d\eta \qquad (31)$$

Algorithm for establishing contact

Curved boundary that can be represented in terms of n-nodded boundary element, as used in boundary element technique as:

$$\left.\begin{aligned} X(\xi) &= \sum_{j=1}^{n} X_j \quad \Gamma_j^n(\xi) \\ Y(\xi) &= \sum_{j=1}^{n} Y_j \quad \Gamma_j^n(\xi) \end{aligned}\right\} \tag{32}$$

Where X_j & Y_j are nodal coordinates of boundary nodes used to define general curved boundary, ξ is the intrinsic coordinate along the boundary and $\Gamma(\xi)$ are the lagragian shape functions.

Let the normal vector from a point (X_i, Y_i) meet the curved boundary of the point $(X_0 \& Y_0)$ then:

$$\left.\begin{aligned} X_0 &= \sum_{j=1}^{n} X_j \; * \; \Gamma_j^n(\xi_0) \\ Y_0 &= \sum_{j=1}^{n} Y_j \; * \; \Gamma_j^n(\xi_0) \end{aligned}\right\} \tag{33}$$

Where X_0, Y_0, ξ_0 are unknown of the parameters.

The derivatives of X and Y with the respect to ξ at (X_0, Y_0) can be written as following:

$$\left.\begin{aligned} \left(\frac{dX}{d\xi}\right)_0 &= \sum_{j=1}^{n} X_j \left(\frac{d}{d\xi}\Gamma_j^n(\xi)\right)_0 = -m \\ \left(\frac{dY}{d\xi}\right)_0 &= \sum_{j=1}^{n} Y_j \left(\frac{d}{d\xi}\Gamma_j^n(\xi)\right)_0 = \imath \end{aligned}\right\} \tag{34}$$

Where $\imath$ & m are directions cosines of outward unit normal vectors at $(X_0 \& Y_0)$

Boundary conditions implementation: If a node i contact the rigid surface for the point $(X_0 \& Y_0)$, then useful to write stiffness equations for that node in terms of normal and tangential components for that the point.

Let direction cosines of normal to the rigid curved surface at $(X_0 \& Y_0)$ be, $\imath \& m$. Then the displacement components along the normal and tangent direction are:

$$\begin{Bmatrix} U_n \\ V_t \end{Bmatrix} = \begin{Bmatrix} \imath & m \\ -m & \imath \end{Bmatrix} \begin{Bmatrix} u \\ v \end{Bmatrix} = [Q] \begin{Bmatrix} u \\ v \end{Bmatrix} \tag{35}$$

And therefore the stiffness matrix is

$$\left[K_Q\right]=[Q]^T\left[K_g\right][Q] \tag{36}$$

Where $[Q]$ is the rotation matrix, as in eq. (35)

Results and Discussion

In this study a poinion with 24 teeth or 36 teeth and with wheel of 36 teeth is considered. The moduls is taken equal to 12mm. The material of the pinion is hardening steel 20 MnCr5 [according to DIN 17210] with the following material properties:

Young of modulus $= 210*10^3\ N/mm^2$

Poisson's of ratio =0.3

$\sigma_{ult} = 1000-1300\ N/mm^2$

$\sigma_y = 700\ N/mm^2$

The finite element mesh problem shown in the figures (1), where 451 element of 4-node solid are employed with either using contact element number 48 or target element 169 with contact element 171.

The boundary conditions for the pair of teeth are given in figure (1), where (Γ_1) is a part of boundary of the investigated domain condition, and all the nodes are constrained in R and $\theta-$ axes i.e. all the nodes lying in this boundary have $UR = U\theta = 0$, while the nodal forces are unknown (Γ_2) represents the loaded boundary condition where an external force of 250N is applied to each of the mesh nodes at the boundary (Γ_2). The effect of inertia force due to acceleration or deceleration.

Referring to figure (2) pinion with center at O_1 is driver and turns counter clockwise. Pressure or generating line is same as the cord used to generate the involute, and contact occurs along this line.

The initial contact will take place when the flank of the deriver comes into contact with the tip of the driven tooth. This occurs at point C_1 in figure (2) where the addendum circle of the driven gear crosses the pressure line. As the tooth goes into mesh, the point of contact will slid up the side of the driving tooth so that the tip of the driver will be in contact just before contact ends. The final point of contact will, therefore, be where the addendum circle of the driver crosses the pressure line. This is point (C_5) in figure (2). The two end points are considered in the analysis as well as other three points which are points C_2 point C_4 and a pitch point C_3 as indicated in figure (3)

The material of the wheel is taken either similar to the poinion's material or is assumed to be very rigid. The main dimensions of the investigated teeth are shown in figure (4) and the geometry of the gear tooth is generated using (AUTOCAD) package, where an exact geometrical relationships (shown in appendix A) are used.

The speed ratio is equal to 1.5 and the Young's modulus of the wheel to the pinion is taken as $E_1/E_2 = 1, 0.8$.

This table is for no-load sheering conditions. i.e. for contact ratio equal to one which is the extreme case. For the actual case when the contact ratio is greater than unity. The load sheering condition is presented and the highest value of the shear stress will be at the beginning and ending of single pair contact, that means $C_2 \& C_4$.

Table 1: Shows the position of maximum shear stress

Contact point	Maximum τ_{xy} Mpa	Depth w mm	Shifting S mm
C_1	889.78	0.5	0.63
C_2	345.64	0.87	0.96
C_3	327.04	0.94	01.15
C_4	324.04	0.83	1.12
C_5	507.68	0.1	0.42

Table 1 gives value of the maximum shear stress and location of the sub-surface points, i.e. the depth (w) and shifting (S) maximum shear stress from the loading point $(\bar{P})$.

Table 2: Shows the position of maximum shear stress

Contact point	Maximum τ_{xy} Mpa	Depth w mm	Shifting S mm
C_1	864.02	0.1	0.28
C_2	338.3	0.68	0.99
C_3	320.5	1.36	1.26
C_4	323.61	1.28	1.14
C_5	474.31	0.1	0.24

Tables 3& 4 show the values of the maximum shear stress, its depth and shifting from the contact point. From table 3&4 it is clear that the maximum depth of the maximum shear stress is at the pitch point. Whilst the minimum value of the maximum shear stresses is at that point. Effluence of $E1/E2$ ratio to the maximum shear stresses is at point C5, is the clear that value of the maximum shear stress for $E1/E2=1$ is 1265 Mpa and it is reduced to 913.98 Mpa for $E1/E2=0.8$. Therefore it is recommended to use $E1/E2$ less than 1 to improve the maximum shear stresses distribution with the pinion teeth, providing that other design requirements are not affected.

Table 3: Shows the position of maximum shear stress

Contact point	Maximum τ_{xy} Mpa	Depth w mm	Shifting S mm
C_1	664.5	0.31	0.54
C_2	406.7	0.5	0.84
C_3	382.58	0.47	0.97
C_4	443.1	0.6	0.74
C_5	1265	0.25	0.31

Table 4: Shows the position of maximum shear stress

Contact point	Maximum τ_{xy} Mpa	Depth w mm	Shifting S mm
C_1	660.4	0.35	0.56
C_2	413.8	0.44	0.87
C_3	386.1	0.57	0.99
C_4	555.2	0.54	0.8
C_5	913.98	0.24	0.4

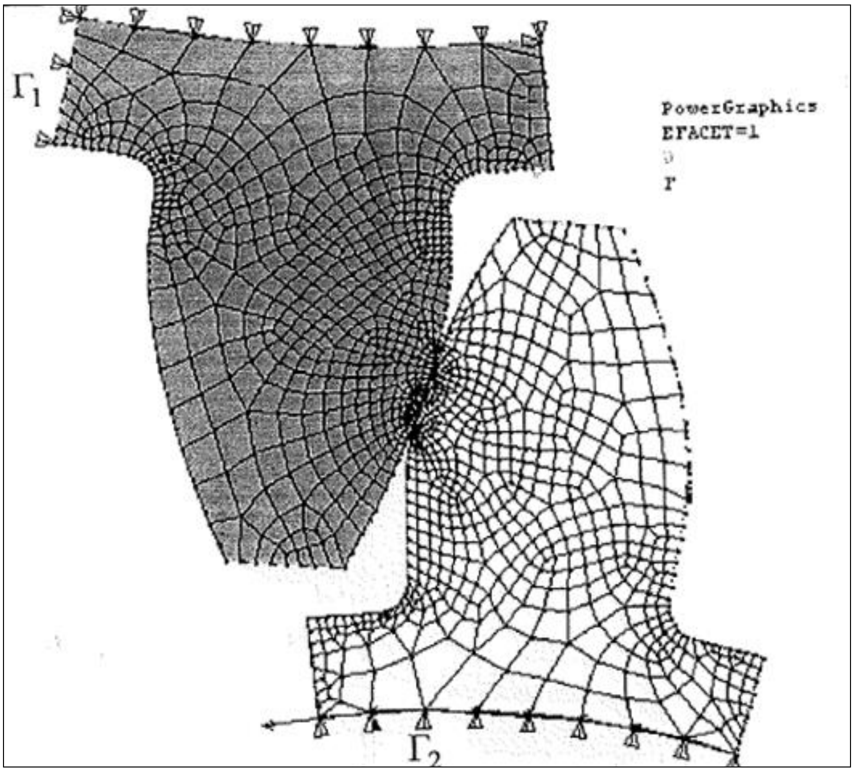

Fig 1: The FE mesh & boundary condition

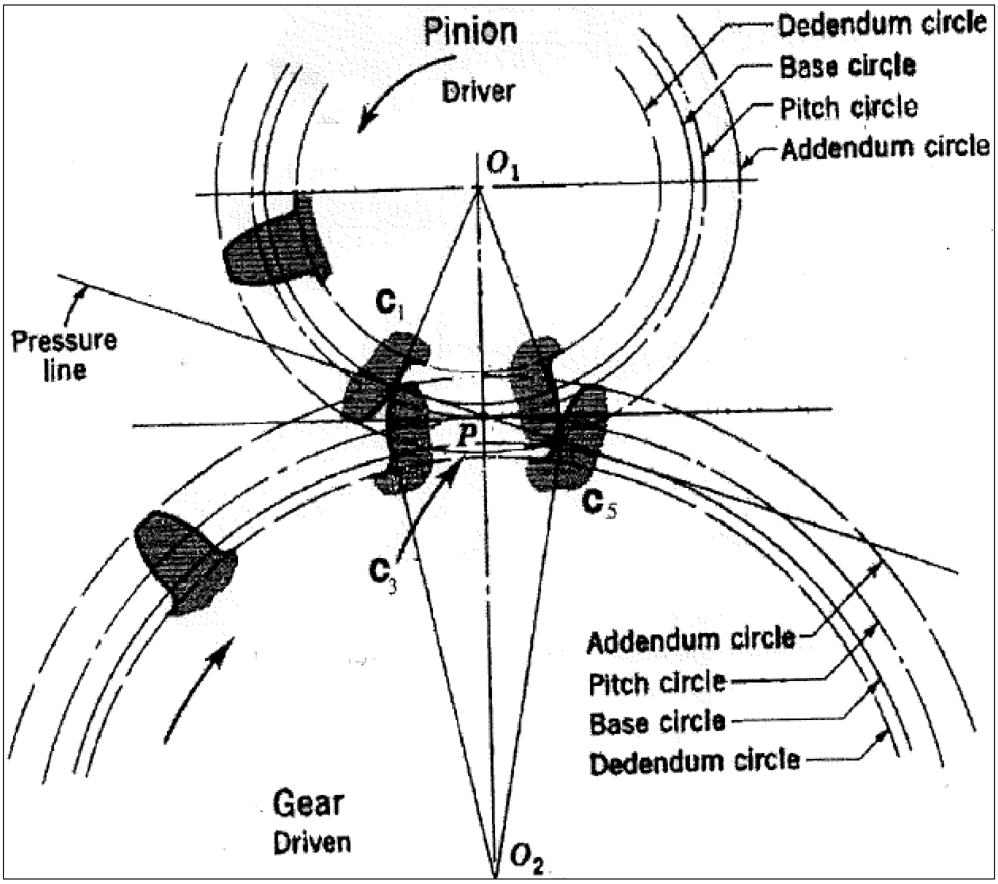

Fig 2: Tooth action

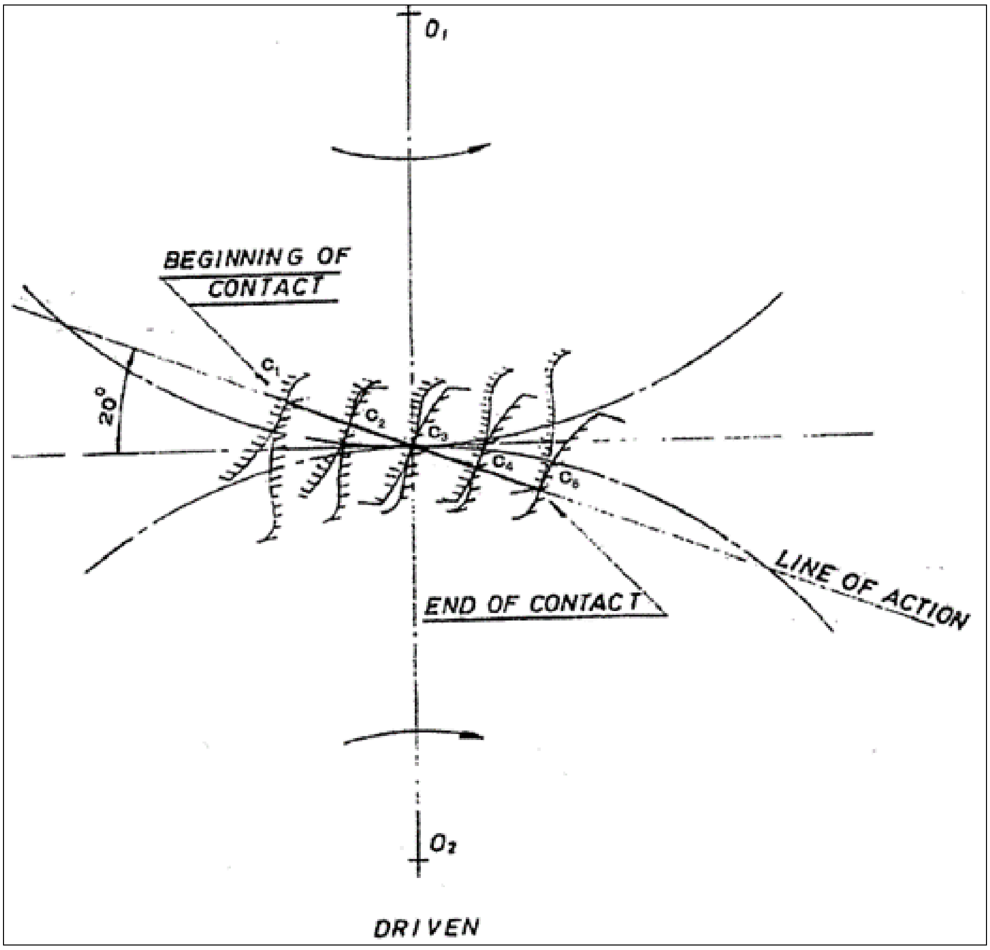

Fig 3: Investigated contact position along the pressure line

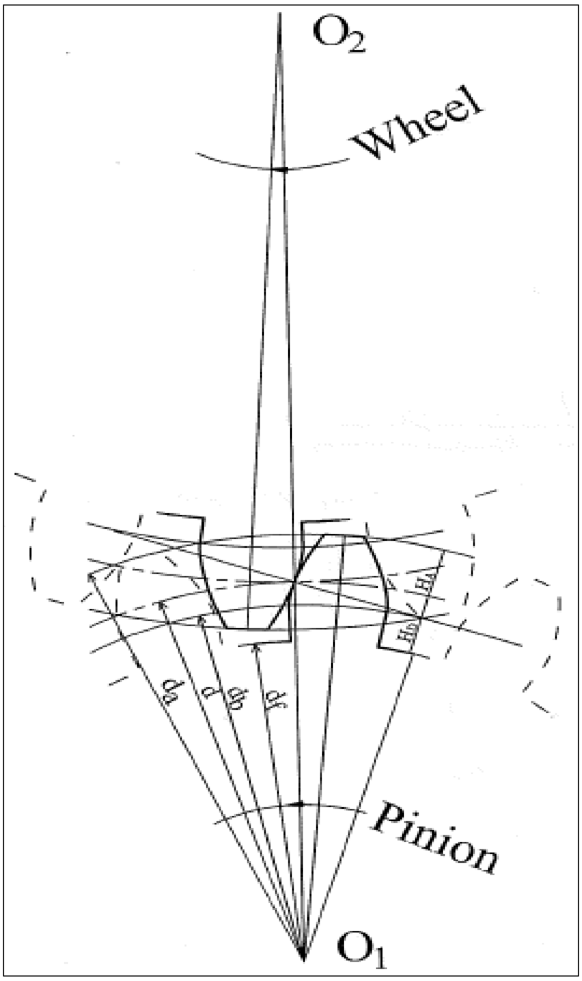

Fig 4: Shows the main dimension for the spur gear

Figure (5.a) shows the shear stress contour at the beginning of contact (i.e. point C_1). Clear that shear stress in pinion is the greater than wheel, this is due to that the radius of curvature of the pinion surface is very small compared to the wheel radius of the curvature. Maximum shear stress is 889 Mpa at point P^*. Depth equal to 0.5mm from surface and it is shifted by 0.63mm to left of the loaded point $\bar{P}$.

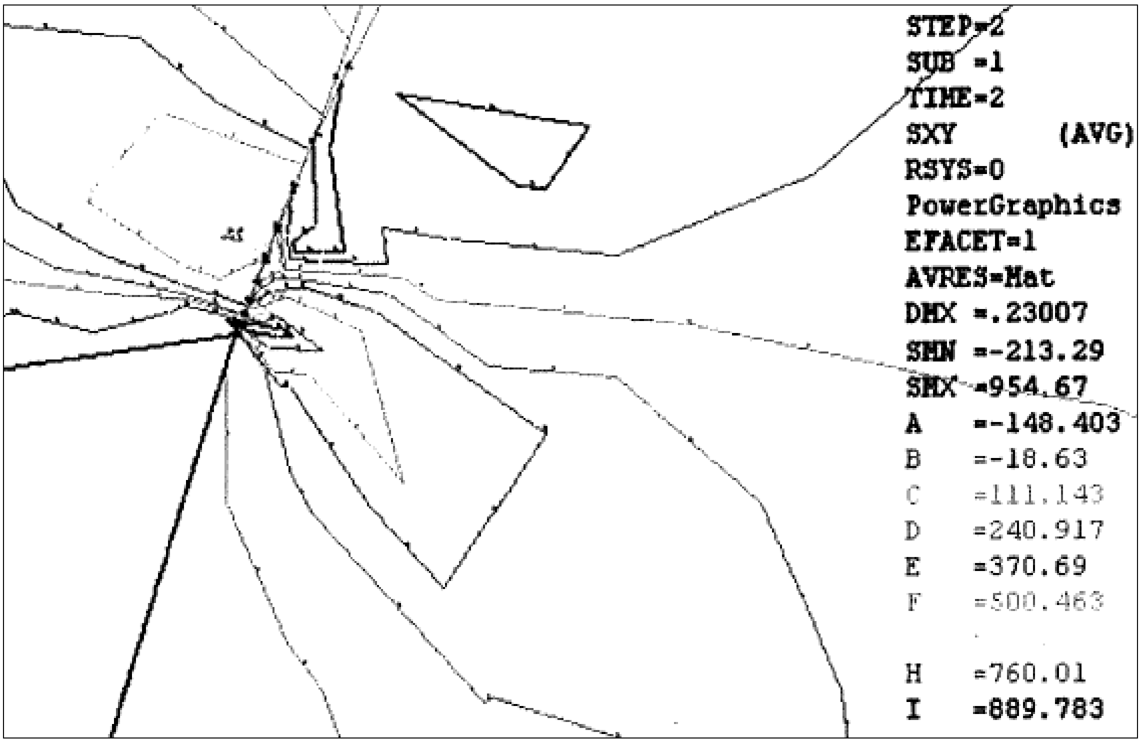

a) Shear stresses contours

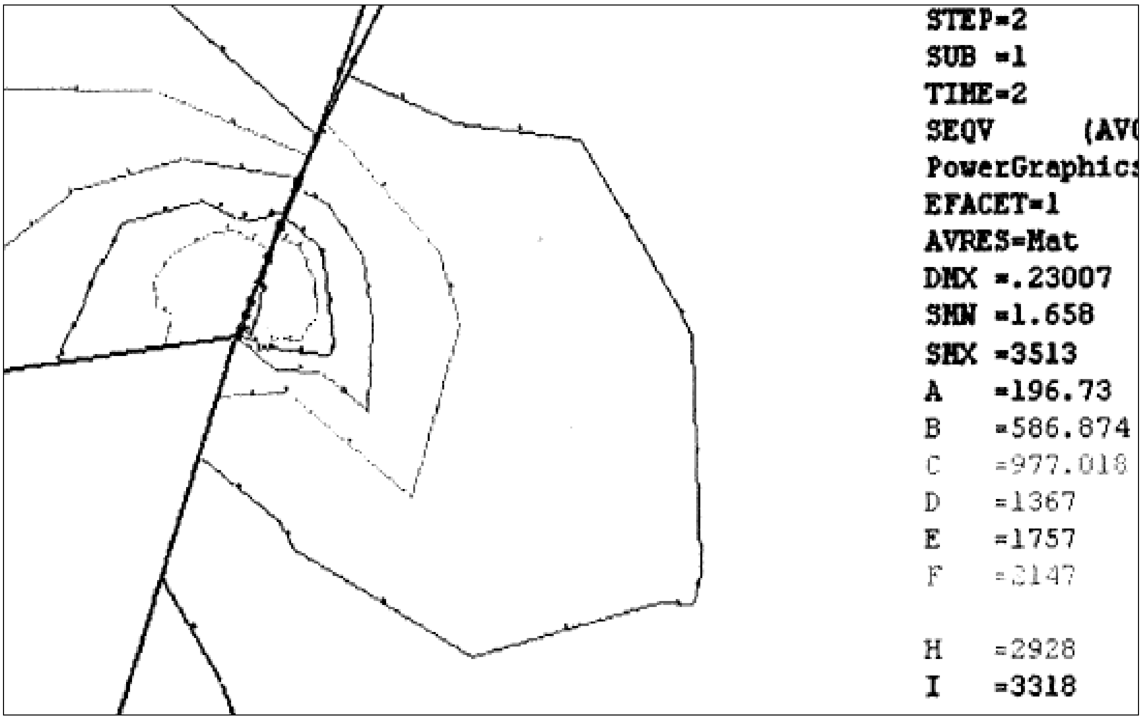

b)Equivalent Von Mises stresses

Fig 5: Stress contours at 1^{st} point (C_1) of contact (m=12, speed ratio 1.5, $E1/E2=1$.

Figure (6.a) shows the contact stress results at contact point C_2 along the pressure line. Maximum shear stress is equal to 345.6 Mpa and it is at the sub-surface of the wheel material by 87 mm. It is unexpected that maximum shear of stress is at the wheel tooth instead of the corresponding pinion tooth. There is great symmetry in the equivalent stress, as indicated in figure (6.b).

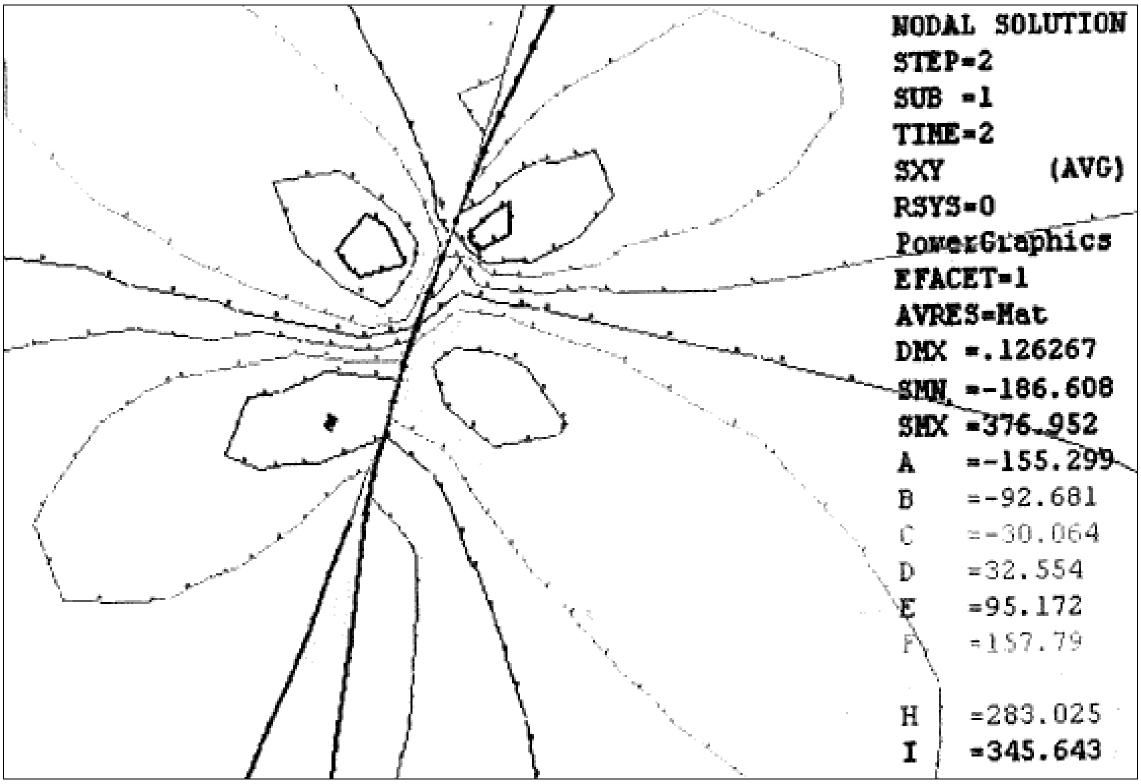

Shear stresses contours

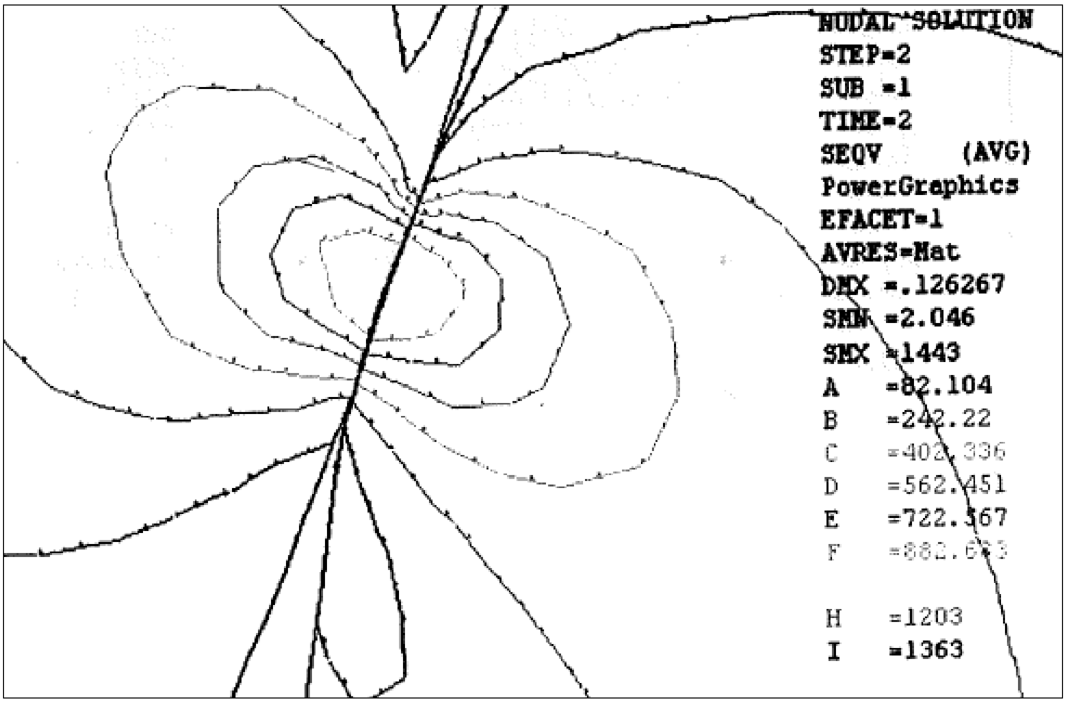

Equivalent Von Mises stresses

Fig 6: Stress contours at 2^{nd} point (C_2) of contact (m=12, speed ratio 1.5, $E1/E2=1$.

Conclusions

A finite element simulation for surface contact stresses of gear teeth is presented. The derivation of the finite element equations is based on elastic large deflection. The main outlines of a finite element solution algorithm and software are given for this purpose, due to the stability and measuring accuracy problems an existing finite element-package (ANSYS) is used. In this study five positions along the contact line are considered to evaluate the contact stress on the pinion and wheel teeth. The influence of speed ratio and the ratio of Young's modulus of the pinion are considered during the investigation. It is found that the maximum shear stress is at the beginning and the end of contact point, therefore the design life calculations of the gear tooth should be based upon these points instead of the pitch point of contact stress in the systemic design calculations.

1. For high value of $(E1/E2)$ I.e. for rigid wheel and elastic pinion, the point of maximum shear stress appeared in pinion tooth for all contact positions along the pressure line. From the view point of design, it is very important to increase the Young's of the pinion material compared to that of the gear, such that to reduce the property of subsurface failure.
2. For using nearly the same materials for the pinion and the wheel or for the case of Young's modulus of the wheel is greater than the Young's modulus of pinion. The maximum shear stress and equivalent Von Mises stress appeared in both wheel and pinion teeth. At the beginning of contact the maximum stress is at the pinion tooth and the maximum equivalent Von Mises is at the wheel tooth. At the ending of contact the maximum equivalent Von Mises is at the pinion tooth.
3. When the speed ratio is increased maximum shear of stress is reduced for all the values of ratio $(E1/E2)$. This is due to the fact the contact stress values have indirect proportionality with the radius of curvature of the contact surface.
4. It is found that the speed ratio has no influence on maximum shear of stress distribution along path of the contact.

References

1. Damtie S, Tilahun D. Contact stress analysis of involute spur gear by finite element method (FEM). Journal of EEA. 2014;32:33-40.
2. Hassan AR. Contact stress analysis of spur gear teeth pair. International Scholarly and Scientific Research & Innovation. 2009;3:1279-1284.
3. Keer LM, Bryant MD. A pitting model for rolling contact fatigue. ASME J Lubr Tech. 1983;105:198-205.
4. Rao PS, Sriraj N, Farookh M. Contact stress analysis of spur gear for different materials using Ansys and Hertz equation. International Journal of Modern Studies in Mechanical Engineering (IJMSME). 2015;7:45-52.
5. Zhai Y, Mu J, Yun R, Jia S, En J, Gao Z, *et al*. Analysis of tooth surface contact stress of involute spur gear. Journal of Physics: Conference Series. 2021;2133:1-6.
6. Ren Z, Glodez S, Flasker J. Influence of inclusion interfaces on surface pitting. Technology Law and Insurance. 1999;4:137-144.
7. Sivakumar K, Manikandan TMS, Balaguru S, Sabarish R, Hariharan R. Contact stress analysis of a spur gear tooth pair for two different materials. International Journal of Applied Engineering Research. 2015;10:344-349.
8. Narayankar ND, Mangrulkar KS. Contact stress and bending stress analysis of spur gear by analytical method. International Journal on Theoretical and Applied Research in Mechanical Engineering (IJTARME). 2017;6:1-3.
9. El-Abbasi N, Meguid SA, Czekanski A. On the modeling of smooth contact surface using cubic splines. International

Journal for Numerical Methods in Engineering. 2001;50:953-967.
10. Balaji DS, Prabhakaran S, Kumar JH. Analysis of surface contact stress for a spur gear of material steel 15Ni2Cr1Mo28. ARPN Journal of Engineering and Applied Sciences. 2017;12:6582-6586.
11. Glodez S, Ren Z, Fajadiga. Computational modeling of the surface fatigue crack growth on gear teeth flanks. Communications in Numerical Methods in Engineering. 2001;17:529-541.
12. Selvam R, Ravi S, Balasubramanian K. Stress analysis of SiC reinforced polyester nanocomposite spur gear. International Journal of Engineering & Technology. 2018;7:305-308.
13. Lei X. Contact friction analysis with a simple interface element. Computer Methods in Applied Mechanics and Engineering. 2002;190:1955-1965.
14. Francvilla OC, Zienkiewicz. A note on numerical computation of elastic contact problems. International Journal for Numerical Methods in Engineering. 1975;9:913-924.
15. Glodez S, Ren Z, Flasker J. Simulation of surface pitting due to contact loading. International Journal for Numerical Methods in Engineering. 1998;43:33-50.